Carbohydrate Polymers 91 (2013) 492–501

Contents lists available at SciVerse ScienceDirect

Carbohydrate Polymers

journal homepage: www.elsevier.com/locate/carbpol

Acrylic acid grafted guargum–nanosilica membranes for transdermal diclofenac delivery

Arindam Giri[a], Tridib Bhunia[a], Samir Ranjan Mishra[b], Luna Goswami[b], Asit Baran Panda[c], Sagar Pal[d], Abhijit Bandyopadhyay[a,*]

[a] Department of Polymer Science and Technology, University of Calcutta, 92 A.P.C. Road, Calcutta 700009, India
[b] KIIT School of Biotechnology, KIIT University Campus-XI, Patia, Bhubaneswar 751024, Orissa, India
[c] Disciplines of Inorganic Materials and Catalysis, Central Salt and Marine Chemicals Research Institute (CSMCRI), Bhavnagar 364021, Gujarat, India
[d] Department of Applied Chemistry, Indian School of Mines, Dhanbad 826004, India

ARTICLE INFO

Article history:
Received 7 June 2012
Received in revised form 20 July 2012
Accepted 9 August 2012
Available online 4 September 2012

Keywords:
Guargum
Graft copolymer
Nanosilica
Diclofenac
Transdermal

ABSTRACT

Green, hydrophobic device for controlled transdermal release of diclofenac sodium was designed from in situ nanosilica/acrylic acid grafted guargum membranes. Best grafting condition was assigned and nanocomposites were formed in situ using varying proportions of aqueous nanosilica sol. Nanocomposite/drug conjugates were formed by bringing down the medium pH from 9.0 to 7.0. The conjugates were characterized through infrared and solid state NMR spectroscopy, electron microscopy, hydro-swelling, surface contact angle, viscometry and biocompatibility. Most balanced property was exhibited by the membrane containing 1 wt% nanosilica. It also had shown the highest encapsulation efficacy vis-à-vis slowest release as compared to others during experimentation in a Franz diffusion cell.

1. Introduction

Membranes based in vitro drug delivery, known as patch therapy (Morrow et al., 2010; Onuki, Nishikawa, Morishita, & Takayama, 2008), has now become highly popular due to reduced side effects, particularly, during prolonged administration. Selection of membranes usually depends on nature of the drug such as its chemical structure and solubility since encapsulation and release is a function of strong drug–polymer interaction (Tomic, Micic, Dobic, Filipovic, & Suljovrujic, 2010). Synthetic, biocompatible membranes made from poly(vinyl alcohol) (Cavalieri et al., 2008; Tortora, Cavalieri, Chiessi, & Paradossi, 2007), poly(acrylic acid) (Adnadjevic, Jovanovic, & Drakulic, 2007; Don et al., 2008), poly(methyl methacrylate) (McCoy, Morrow, Edwards, Jones, & Gorman, 2007), poly(ethylene glycol) (Yu & Pishko, 2011), etc. and their derivatives (Lee & Chen, 2006; Sullad, Manjeshwar, & Aminabhavi, 2010; Zhou & Faust, 2005) are usually preferred for encapsulating most of the drugs as (i) they can produce specific interaction with the drug molecules and (ii) they have strong ability to form free standing membranes.

Biodegradability and other environmental issues, for the last 10–15 years, have stipulated use of biopolymer made membranes as an alternative to synthetic ones. Several biopolymer membranes, mainly cellulose (Butun, Ince, Erdugan, & Sahiner, 2011) and carbohydrate based (Frutos, Prior-Cabanillas, París, & Quijada-Garrido, 2010; Santos, Veiga, Pina, & Sousa, 2005), have been developed and characterized so far for different drug delivery applications but their low matrix coherency owing to weaker strength and elongation is still a major concern for high success rate.

The present project targets to design suitable biopolymer membranes for encapsulation and controlled release of diclofenac sodium. Diclofenac is the commonest drug prescribed for rheumatoid arthritis and other joint ailments (Altman & Barkin, 2009; Banning, 2006). Protracted intake produces several side effects like severe gastro-intestinal and renal dysfunction (Wang et al., 2004). The half life is very short, only 2.5 h, and it has poor water solubility (soluble within pH 6.0–7.0). The later is due to the presence of hydrophobic phenyl rings in its chemical structure (supplied as Supplementary figure). Topical formulation containing 1% diclofenac is commercially available but it is never recommended when extended therapy is in demand. So far we have developed series of biopolymer nanocomposites involving carboxymethyl guargum (CMG) and functionalized multiwalled carbon nanotube (Giri, Bhowmick, Pal, & Bandyopadhyay, 2011) and nanosilica (Giri, Ghosh, Panda, Pal, & Bandyopadhyay,

* Corresponding author. Tel.: +91 033 23501397 6996/6387/8386x288.
E-mail addresses: abhijitbandyopadhyay@yahoo.co.in, abpoly@caluniv.ac.in (A. Bandyopadhyay).

0144-8617/$ – see front matter © 2012 Elsevier Ltd. All rights reserved.
http://dx.doi.org/10.1016/j.carbpol.2012.08.035

2012) to improve membrane stability vis-à-vis to ease on-site matrix–diclofenac interaction. Some previous reports described use of hydroxypropyl methyl cellulose (El-Leithy, Shaker, Ghorab, & Abdel-Rashid, 2010) and carbpol 934 (non-specific carbohydrate) where 60% of the loaded diclofenac was maximally retained (40% release) after 6 h study. Conversely, our latest device from CMG/nanosilica was able to retain 68% diclofenac (32% release) even after 20 h observation (Giri et al., 2012). Two factors: (i) viscosity and (ii) hydrophobicity were dominating parameters for better encapsulation and release. In our subsequent efforts we have tried to work on these for better outcome.

The matrix selected for present investigation was guargum (GG) as it is less hydrophobic than CMG. Prabaharan (2011) in a recent review has discussed prospects of guargum and its various derivatives as drug delivery device including transdermal application. We have modified GG with acrylic acid to develop novel graft copolymers inside nanosilica sol for intimate polymer–silica contacts to raise membrane stability. Some of the former studies discussed about the use of variously grafted guargum (George & Abraham, 2007; Krishnaiah, Karthikeyan, & Satyanarayana, 2002; Thakur, Chauhan, & Ahn, 2009) as ordinary hydrogels mostly for oral drug delivery application but none of them and many others published before had described release behavior of diclofenac. Free radical grafting of acrylic acid on GG has not been widely investigated excluding only one earlier report by Huang et al. on photoinitiated acrylic acid grafting on cationic guar gum in 2007 (Huang, Yu, & Xiao, 2007). In the first step, the grafting conditions were optimized for highest grafting yield. Nanocomposites were prepared in situ with the best copolymer in the second step and the membranes were cast. The dry membranes were subsequently characterized for matrix–silica adhesion. Pathogenic and non-pathogenic microbial activities were conducted over the nanocomposites to test the biocompatibility. Drug elution was monitored through a Franz diffusion cell. Results were fitted to standard kinetic models for analysis.

2. Experimental

2.1. Materials

GG was kindly supplied by Hindustan Gum and Chemicals Ltd., Haryana, India. Aqueous nanosilica sol (25% silica content, average size 13 nm) stabilized at pH 9.0 was generously supplied by Bee Chem, Kanpur, India. Acrylic acid (AA, 99% pure), potassium persulphate ($K_2S_2O_8$) and hydroquinone, all of standard laboratory grade, were purchased from Loba Chem., Mumbai, India. Diclofenac sodium was the gift sample received from Ranbaxy Int. Gurgaon, Haryana, India.

2.2. Acrylic acid grafting and in situ drug encapsulated nanocomposite synthesis

Graft copolymerization was done free radically by using $K_2S_2O_8$ as the grafting initiator. One AGU (anhydro glucose unit) of GG was dissolved in 50 ml distilled water taken at pH 9.0 with constant stirring and bubbling low stream nitrogen for 15 min. Desired AA as sodium acrylate at pH 9.0 was added and nitrogen was purged for another 30 min. Aqueous $K_2S_2O_8$ was added and the temperature was raised to 75 °C. The reagents were allowed to react for 3 h under nitrogen. The reaction was quenched by adding adequate saturated hydroquinone. The kettle temperature was lowered to 30 °C and the whole mass was allowed to stand overnight. One night later, the reaction mass was adjusted to pH 7.0 and poured into excess acetone to settle down the graft copolymers. The mass was carefully filtered, washed three times with acetone and finally vacuum dried to drive off all absorbed acetone. The hard mass was pulverized, sieved and finally dissolved in water forming GG-g-AA sol. The copolymer yield was compared at various initiator and monomer compositions, for optimization (Table 1). In situ nanocomposites were synthesized using best reaction conditions at different nanosilica concentrations, detailed in Table 1. The whole process was repeated as stated up till sol formation. Diclofenac was added in equal proportion (1 mg) to all nanocomposites and ultrasonicated for 15 min to ensure adequate drug–nanocomposite mixing. Subsequently, the sols were thinly cast on Teflon sheet for gelation into membrane. Average thickness of the membranes was 0.25 mm.

2.3. Characterization

The grafting yield (in percent) was calculated using Eq. (1):

$$\text{Grafting yield (\%)} = \left(\frac{\text{wt. of the reactant mixture} - \text{wt. of the dry sample after ppt.}}{\text{wt. of the reactant mixture}}\right) \times 100 \quad (1)$$

Spectroscopic characterization of grafted and nanocomposite membranes were done through Fourier transform infrared (FTIR) spectrophotometer, JASCO FTIR, within the spectral range of 400–4000 cm^{-1} and resolution 4 cm^{-1} and solid state ^{13}C nuclear magnetic resonance (NMR) spectrophotometer (Bruker, 500 MHz) under ambient condition. Thermal stability from room temperature (27 °C) to 600 °C was tested in a thermogravimetric analyzer (TGA) Perkin Elmer, using a heating rate of 10 °C/min under nitrogen. Morphology of the nanocomposite was viewed under a transmission electron microscope (TEM, C-12, Philips) operated at 400KV. Nanocomposite sols, diluted by 1000 times, was cast on copper grid of 300 mesh and then dried in an oven and finally placed under TEM for analysis. Silica dot mapping was produced from a scanning electron microscope (SEM, JEOL, JSM 5800) operated at 15 kV. Hydro-swelling study of the nanocomposites was done by periodical weighing of the membranes, immersed in water, after soaking all the surface water. The data were plotted as swelling ratio against time interval to understand the water absorption kinetics. Hydrophobic/hydrophilic balance of the membranes was assessed by measuring air–water contact angle of a sessile water drop (double distilled) in a contact angle meter (Kernco, Model G-II, EI Paso, TX, USA) after its equilibrium spreading over microscopically smooth and dirt free membrane surface. Rheological measurements were made in a HAAKE Viscotester 550, Thermo Scientific, Germany within the shear rate range of near zero to 400 s^{-1} under ambient.

Biocompatibility of the membranes was assessed by observing microbial growth over the membrane mass used as the substrate. The normal LB agar based media was prepared by mixing 10 g tryptone (E-Merck, Germany), 5 g of yeast extract (E-Merck, Germany), 5 g of sodium chloride (HiMedia, India) and 1 l distilled water. The pH was adjusted to 7.5 by using 1 N HCl and N/10 NaOH (approximately). The mass was stirred for 30 min for homogenization. Fifteen grams agar–agar (Merck) was added to it and mixed thoroughly. 25 ml of the media was mixed with 2% nanocomposite dispersion to make 5:1 (media:composite) combination. Each combination was autoclaved at 120 °C and 15 psi for 15 min and then spread into petri plates under sterile condition at 40 °C. The plates were allowed for solidification. Each nanocomposite was used to grow 6 different bacterial stains such as *Salmonella typhii*, MTCC 96 (*Salmonella aureus*), E. Coli (*Escherichia coli*), Bacillus, SEN 125 (*Salmonella enteritdis*) and SB 300 (*Salmonella typhimurium*). The agar media–composite plates and the control plate (without composite) were kept in an incubator at 37 °C for 72 h. The pictures of the plates were taken after 72 h of observation.

Table 1
Sample composition and designation, carbonyl group (C=O) peak area ratio, standard FTIR transmittance peaks of GG, contact angle measurement and drug release kinetic fitting data.

Hydrogel designation	Guargum (GG) mole	Acrylic acid (AA) mole	Initiator Concentration (wt%) w.r.t. AA	Nanosilica (wt%) w.r.t. total mass	C=O peak area ratio (1705/2983)	GG peak transmittance (cm^{-1})	Corresponding functionality	Contact angle (°)	Zero-order r^2	First-order r^2	Higuchi r^2	Korsmeyer–Peppas	
												r^2	n
GG	1	0	0	0		3278.00	—OH str.		0.90551	0.82333	0.97964	0.97276	0.52079
GG-g-$AA_{2/0.1}$	1	2	0.1	0		2874.68	—C—H str.						
G G-g-$AA_{5/0.1}$	1	5	0.1	0		1648.38	—OH bend.						
GG-g-$AA_{20/0.1}$	1	20	0.1	0		1135.75	—CO str.						
GG-g-$AA_{10/1.0}$	1	10	1.0	0		1016.80	CH—O—CH str.						
GG-g-$AA_{10/0.5}$	1	10	0.5	0		873.84	CH—O—CH str.						
GG-g-$AA_{10/0.1}$	1	10	0.1	0				30	0.95714	0.87101	0.99320	0.98996	0.65928
GG-g-$AA_{10/0.1/0.5}$	1	10	0.1	0.5	0.97053			32	0.97336	0.89502	0.99265	0.99427	0.71916
GG-g-$AA_{10/0.1/1.0}$	1	10	0.1	1.0	0.96338			52	0.99204	0.91589	0.98940	0.99867	0.76495
GG-g-$AA_{10/0.1/3.0}$	1	10	0.1	3.0	0.96480			42	0.98592	0.92621	0.99170	0.99875	0.70239
GG-g-$AA_{10/0.1/5.0}$	1	10	0.1	5.0	0.96760			45	0.97486	0.89334	0.99512	0.99542	0.69336

Transdermal drug release experiment was carried out in a Franz diffusion cell. Detail description of the procedure related to release analysis has been described in our earlier publication (Bhunia, Goswami, Chattopadhyay, & Bandyopadhyay, 2011). Eluted diclofenac was spectrophotometrically analyzed at 276 nm (λ_{max}) after consulting a standard calibration curve.

3. Results and discussion

3.1. Characterizing GG-g-AA copolymers

3.1.1. Effect of initiator concentration

Three persulphate concentrations, 0.1, 0.5 and 1 wt% with respect to AA in 1:10::GG:AA reaction mass were used for optimization. Weight of 1 AGU was taken as the molar weight of GG for reactant calculation. Gravimetric grafting yield at three persulphate contents are compared in Fig. 1a. Highest yield (138%) was achieved at 0.1% (GG-g-$AA_{10/0.1}$) persulphate content while at other levels, the yield was far too less. Low persulphate probably induced more acid radicals for grafting but at higher concentration, the yield diminished due to concurrent poly(acrylic acid) formation. More poly(acrylic acid) formed at higher persulphate concentration visually heterogenized the reaction mass. It was separated during precipitation.

Macromolecular dimension usually changes on grafting. Such changes could be identified through reduced viscosity (η_{sp}/c) measurement. Each viscosity data are plotted against respective persulphate concentration in Fig. 1a to complement grafting yield. All the copolymers showed higher reduced viscosities than virgin for achieving higher hydrodynamic volume. The trend shows highest viscosity for GG-g-$AA_{10/0.1}$ followed by GG-g-$AA_{10/0.5}$ and GG-g-$AA_{10/0.1}$ corroborating respective grafting yield data.

Microstructural evidence of grafting was obtained from strong infrared peak transmittance at 1705 cm^{-1} (FTIR spectra in Fig. 1b) representing antisymmetric and symmetric C=O stretches of the pendant acid unit in GG. The other characteristic peaks of GG are listed in Table 1. The grafting site on GG is preferably β carbon unit of pyranose ring which first opens up and accommodates the initiator bound acid radical (Fig. 2). The other ring carbon concurrently converts into aldehyde upon proton elimination but it is difficult to trace since it is almost inseparable from the grafted acid C=O due to strong overlapping. However, the complementary acid C—O peak, which appeared as inflation at 1170 cm^{-1} along with ethereal C—O—C peak became more prominent in the grafted samples than its weak occurrence at 1134 cm^{-1} in the virgin. Similarly, other sharper and shifted peak transmittances in the graft copolymers appeared at 812 and 1030 cm^{-1} which were originally positioned at 847 and 1016 cm^{-1}. These peaks are for CH—O—CH bond stretches. The peak at 2983 cm^{-1} (C—H stretching) also became prominent after grafting relative to its original emergence, owing to polymerized (alkyl) acid units. The ratio of the peak area of the peaks at 1705–2983 cm^{-1} in each grafted sample was calculated for approximating acid concentrations (carbonyl index). Values are reported in Table 1. GG-g-$AA_{10/0.1}$ had received highest peak area ratio for its maximum grafting yield. Both GG-g-$AA_{10/0.5}$ and GG-g-$AA_{10/1.0}$ had received slightly lower values due to lower yield.

The proposed grafting mechanism was assessed through ^{13}C NMR spectroscopy (Fig. 1c). Neat GG showed three distinct resonances at 103, 73 and 64 ppm for its anomeric carbon, pyranose ring carbon excluding anomeric carbon and carbon atom of CH_2OH unit. However, the spectrum of maximally grafted sample (GG-g-$AA_{10/0.1}$) had shown five distinct resonances at 179.2, 103.1, 73, 63.4 and 43.8 ppm of which the peaks at 63.6, 73 and 103.1 ppm were the pre-assigned peaks of neat GG. New peak at 179.2 ppm indicates the presence of "coalesced" carbonyl carbon of both COOH and

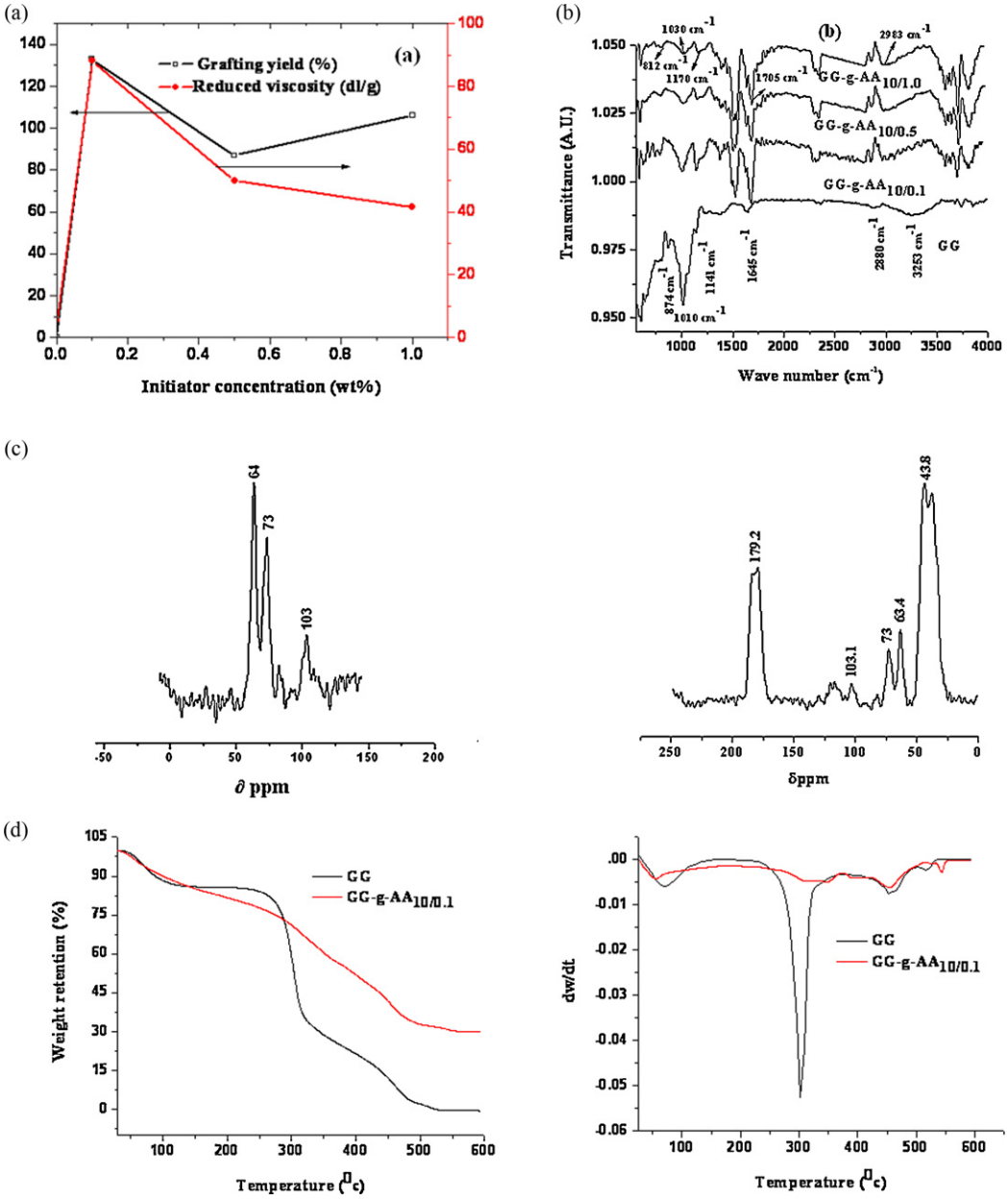

Fig. 1. (a) Grafting yield and reduced viscosity, (b) normalized FTIR spectra at different $K_2S_2O_8$ content in graft copolymer, (c) represents ^{13}C solid state NMR spectrum and (d) demonstrates TG and DTG plots of GG and GG-g-$AA_{10/0.1}$.

CHO where the latter was formed on pyranose ring opening during persulphate mediated graft copolymerization (Fig. 2). Resonance at 45 ppm was responsible for sp3 carbon atoms of the polymerized acid units.

Effect of grafting on thermal degradation of GG is demonstrated in Fig. 1d. Between 150 and 300 °C, weight retention (%) was lower in the grafted sample than GG as it showed steady and continuous decrease in weight retention (%) since beginning of the experiment. But beyond 300 °C, GG recorded drastic weight loss of nearly 55% within next 20 °C (320 °C) followed by the complete degradation loss (0% retention) before 500 °C. Conversely, the grafted sample showed a slow but steady weight loss up to 500 °C and finally retained 30% of its original weight till end of the experiment.

3.1.2. *Effect of acrylic acid concentration*

Effect of AA concentration on grafting was investigated using different GG:AA mole ratios c.a. 1:2, 1:5, 1:10 and 1:20 at fixed persulphate level (0.1 wt%). Data on 1:10 GG:AA was already described in the preceding section. The grafting yield at different acid contents is compared in Fig. 3a. Grafting steadily increased up to 10 times' molar AA content of GG and then declined and finally at 20 times, the yield sharply reduced. Rise in AA produced more free radicals for grafting but in unison also produced more poly(acrylic acid) in the medium. Haul between these dissimilar kinetics strongly deviated the grafting yield values from linearity (Fig. 3a). Thus beyond 1:10 mole ratio, the homo-polymerization reduce grafting yield. Reduced viscosity trend in Fig. 3a also leads to similar conclusion.

Strong symmetric and anti symmetric infrared C=O stretching in Fig. 3b gave microstructural evidence of grafting. Peak intensity ratios at 1705/2983 cm^{-1} in Table 1 quantifiably expressed increasing trend toward polar group insertion (both COOH and CHO) from GG-g-$AA_{2/0.1}$ until GG-g-$AA_{10/0.1}$ and then a downfall for GG-g-$AA_{20/0.1}$.

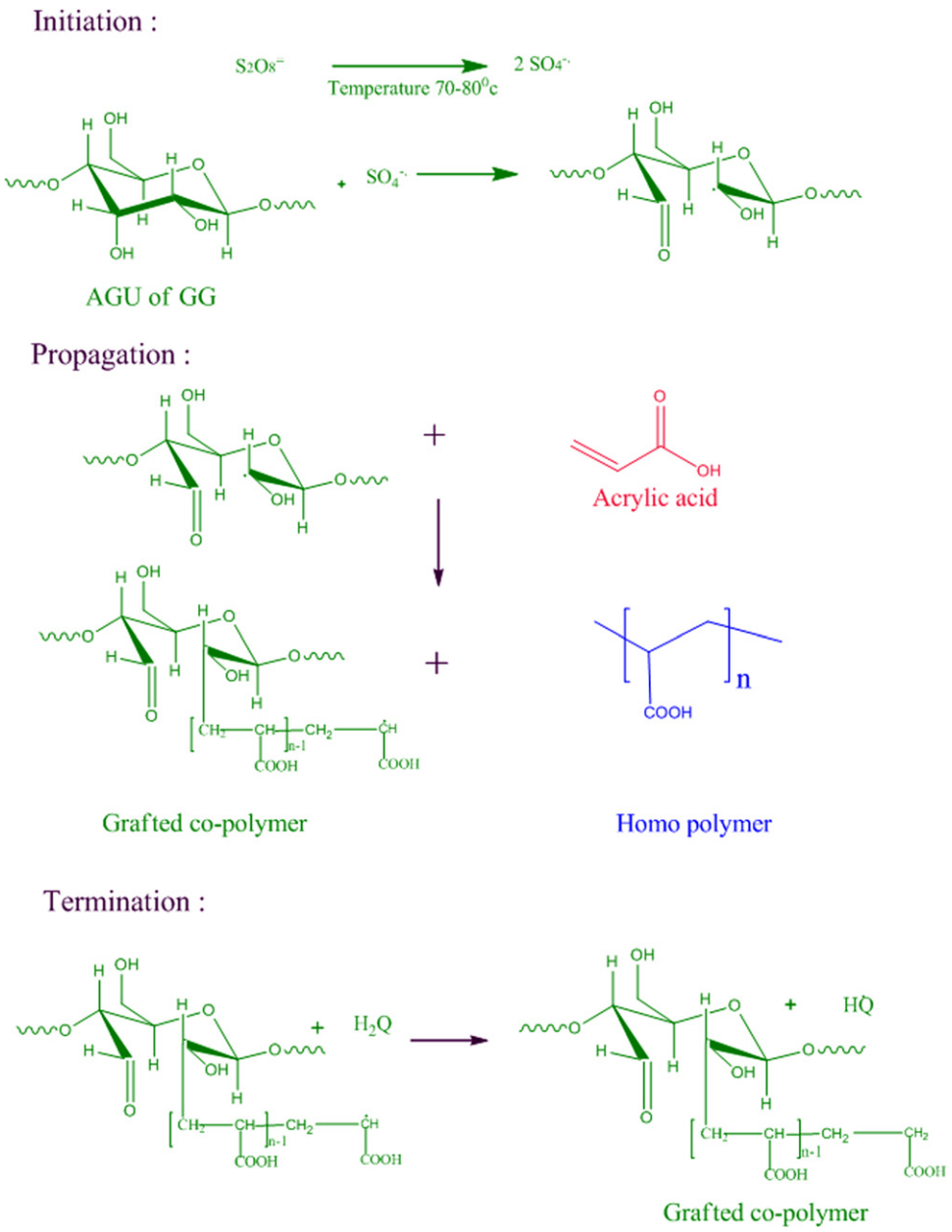

Fig. 2. Mechanism of acrylic acid grafting on guar gum.

3.2. Studies on in situ nanocomposite membranes

3.2.1. Microstructure and morphology analysis

Our sample for nanocomposite synthesis was GG-g-$AA_{10/0.1}$ since it contains maximum grafted units. Normalized FTIR spectra of all nanocomposites are compared in Fig. 4. Si—O—Si asymmetric stretch (silica) normally appears within 1000–1100 cm^{-1} (Bandyopadhyay, Bhowmick, & De Sarkar, 2004) but here it had overlapped with strong C—O—C and C—O stretchings' from both copolymer and drug molecule which made it hard to discriminate. However, silica domains were nicely detected through energy dispersive silicon dot mapping shown in Supplementary figures beside each FTIR spectrum in Fig. 4. The white dots are positions of silica particles whose concentration increased with increasing silica content. At 3 and 5 wt%, the domains were locally concentrated, attributed to condensation between free silanol groups of silica leading to aggregation. TEM images in Fig. 5a and b accurately measured these aggregates as 250 and 290 nm, which are eventually 200 times larger than their original size (13 nm). Aggregation resulted into weaker transmission shift of only 2 cm^{-1} for C=O peak (1705 cm^{-1}) due to poor matrix–silica adhesion. On contrary, 10 and 14 cm^{-1} of sharp transmission shifts toward lower energy realm were evident in GG-g-$AA_{10/0.1/0.5}$ and GG-g-$AA_{10/0.1/1.0}$ owing to strong hydrogen bonded interaction between uncondensed silanol groups-grafted acids and encapsulated drug molecules for finer silica networking (average silica size is 35 nm in GG-g-$AA_{10/0.1/1.0}$ measured from its TEM image in Fig. 5c). Each embedded nanoparticles (mostly size <100 nm) in the network were essentially copolymer capped since viscoelastic domains always adsorbed over harder units in a hybrid system (Bandyopadhyay, De Sarkar, & Bhowmick, 2005). Drug molecules were likely to be trapped inside these networks as demonstrated

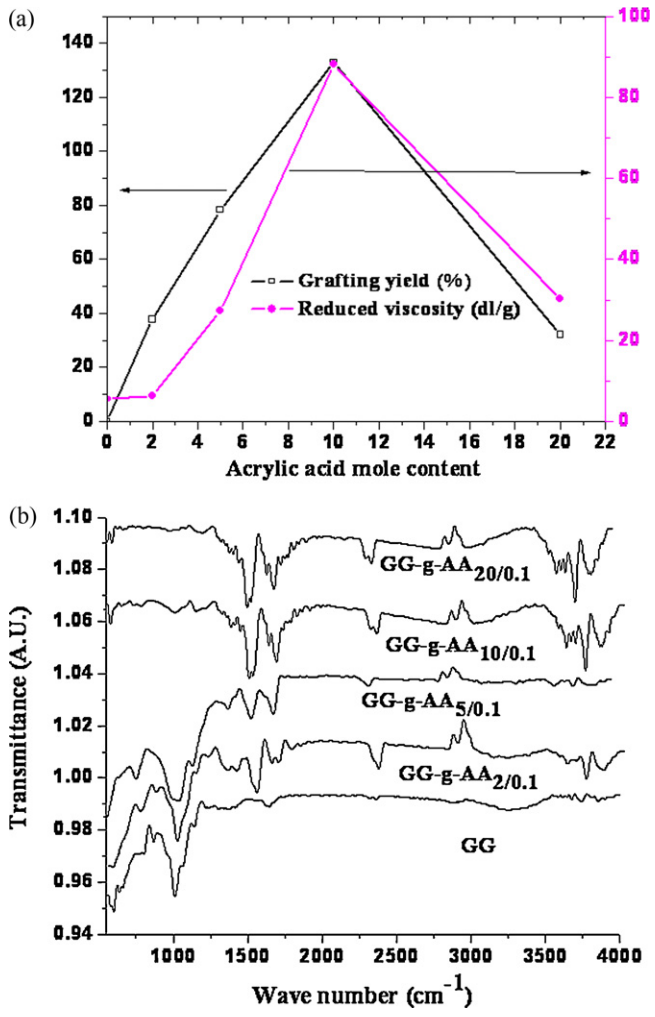

Fig. 3. (a) Grafting yield and reduced viscosity and (b) Normalized FTIR spectra of graft copolymers at different acrylic acid contents.

in Fig. 5d. Adsorptive copolymer–silica interaction also affected alkyl peak shift (C—H stretches) at 2983 cm^{-1}. More aggregation led to low adsorbate area and thus poor peak shifts were observed with both GG-g-$AA_{10/0.1/3.0}$ and GG-g-$AA_{10/0.1/5.0}$ whereas finer silica networking led to better adsorption and thus higher peak shifts were noted in GG-g-$AA_{10/0.1/0.5}$ and GG-g-$AA_{10/0.1/1.0}$. NMR data also produced more de-shielded peak resonances for both alkyl and carbonyl carbons in the GG-g-$AA_{10/0.1/1.0}$/silica/drug conjugate (Fig. 6a) reiterating better matrix silica adhesion than when there was no silica added to the system (Fig. 1c).

3.2.2. Hydro-swelling study

Hydro-swelling kinetics of different nanocomposites is compared in Fig. 6b. GG-g-$AA_{10/0.1/0.5}$ had displayed fastest water intake followed by GG-g-$AA_{10/0.1}$, GG-g-$AA_{10/0.1/5.0}$, GG-g-$AA_{10/0.1/3.0}$ and GG-g-$AA_{10/0.1/1.0}$. Silica nanoparticles and GG-g-$AA_{10/0.1}$, both were highly hydrophilic components in GG-g-$AA_{10/0.1/0.5}$/drug conjugate since number of silanol groups on discrete nanosilica particles was probably far more than the grafted sites of the matrix to interact owing to less self-condensation and that had left more polar groups free to attract huge amount of water at an enormous rate. Conversely, GG-g-$AA_{10/0.1/1.0}$ contained stronger matrix–filler interfaces and generated more copolymer-capped immobile, hydrophobic conjugates (since silanol groups are engaged with pendant acid units) (Bhunia et al., 2011) which were difficult to swell. Swelling kinetics of both GG-g-$AA_{10/0.1/3.0}$ and GG-g-$AA_{10/0.1/5.0}$ were faster than GG-g-$AA_{10/0.1/1.0}$ especially at the latter stages. Reduced interaction between aggregated silica and grafted copolymer catalyzed macro phase separation where the exposed matrix eventually inducted faster water uptake.

Hydrophobic/hydrophilic trend of the nanocomposite conjugates was reconfirmed from air–water contact angles. These are reported in Table 1. Conjugate from GG-g-$AA_{10/0.1/0.5}$ had shown lowest angle of contact implying that it was the most hydrophilic and thus least hydrophobic as compared to the conjugate from GG-g-$AA_{10/0.1/1.0}$ which incidentally showed the highest contact angle indicating its poorest water attracting surface (i.e. most hydrophobic). Rest of the composites followed their hydro swelling trend.

3.2.3. Rheological study

Solution viscosities at various shear rates are displayed in Fig. 6c. The present nanocomposite conjugates are far less viscous than the system we developed previously using CMG and nanosilica (Giri et al., 2012). In present set of samples, low shear viscosities displayed a trend—conjugates with high silica content show higher viscosity than the virgin, may be due to more solubilized copolymer fragment coming from the phase separated conjugates. GG-g-$AA_{10/0.1/1.0}$–drug conjugate had recorded even lower viscosity than GG-g-$AA_{10/0.1}$ since it was exceptionally hydrophobic. Never the less, all nanocomposite conjugates including GG-g-$AA_{10/0.1}$ were pseudo plastic as their viscosity reduced with rising shear rate. The extent to which the viscosities drop (dewetting) and their equilibrium value, both physically demonstrated matrix–silica adhesion gradient. Despite low initial viscosity, GG-g-$AA_{10/0.1/1.0}$–drug conjugate displayed minimum viscosity loss while the loss was highest with GG-g-$AA_{10/0.1/5.0}$ despite its highest low shear viscosity. The behavior was nearly identical in conjugates from GG-g-$AA_{10/0.1/3.0}$ and GG-g-$AA_{10/0.1/0.5}$ but finally the later retained higher equilibrium viscosity due to stronger interface.

3.2.4. Biocompatibility study

Microbial growth potentials of GG-g-$AA_{10/0.1}$ and its hybrid conjugates were imaged and compared in Fig. 7a. Each sample plate was divided in six domains to detect growth volume of individual stains. The stains were clockwisely placed from (1) *Salmonella typhii*, (2) *Salmonella aureus*, (3) *Escherichia coli*, (4) Bacilus, (5) *Salmonella enteritdis*, to (6) *Salmonella typhimurium*. Bacilus is non-pathogenic, while rest five stains are pathogenic. Despite high hydrophilicity, growth volume was drastically low in GG-g-$AA_{10/0.1}$ from control (agar agar) equally with all six stains due to exorbitant synthetic content (high grafting yield). But growth volume increased in all nanocomposite conjugates despite low hydrophobicity and diclofenac content, i.e. all six stains were equally potent in using those nanocomposites as nutrient media. Higher growth volume at higher silica loading (3 and 5 wt%) is another interesting fact noted from these images. Drop in synthetic content (grafted matrix) is the primary reason for higher growth volume despite diclofenac content in the nanocomposites. The secondary reason could well be that, nanosilica particles acted as additional nutrient media for growth. All conjugates were thus "limitedly" biocompatible as their growth potential was well below than control. This is a unique feature since; otherwise, nanocomposites serving as excellent nutrient media would have adversely affected its long-term aerial exposure during therapeutic action.

3.2.5. Drug delivery analysis

Drug delivery potentials of neat GG, GG-g-$AA_{10/0.1}$ and all nanocomposite conjugates are compared in Fig. 7b. Both GG and

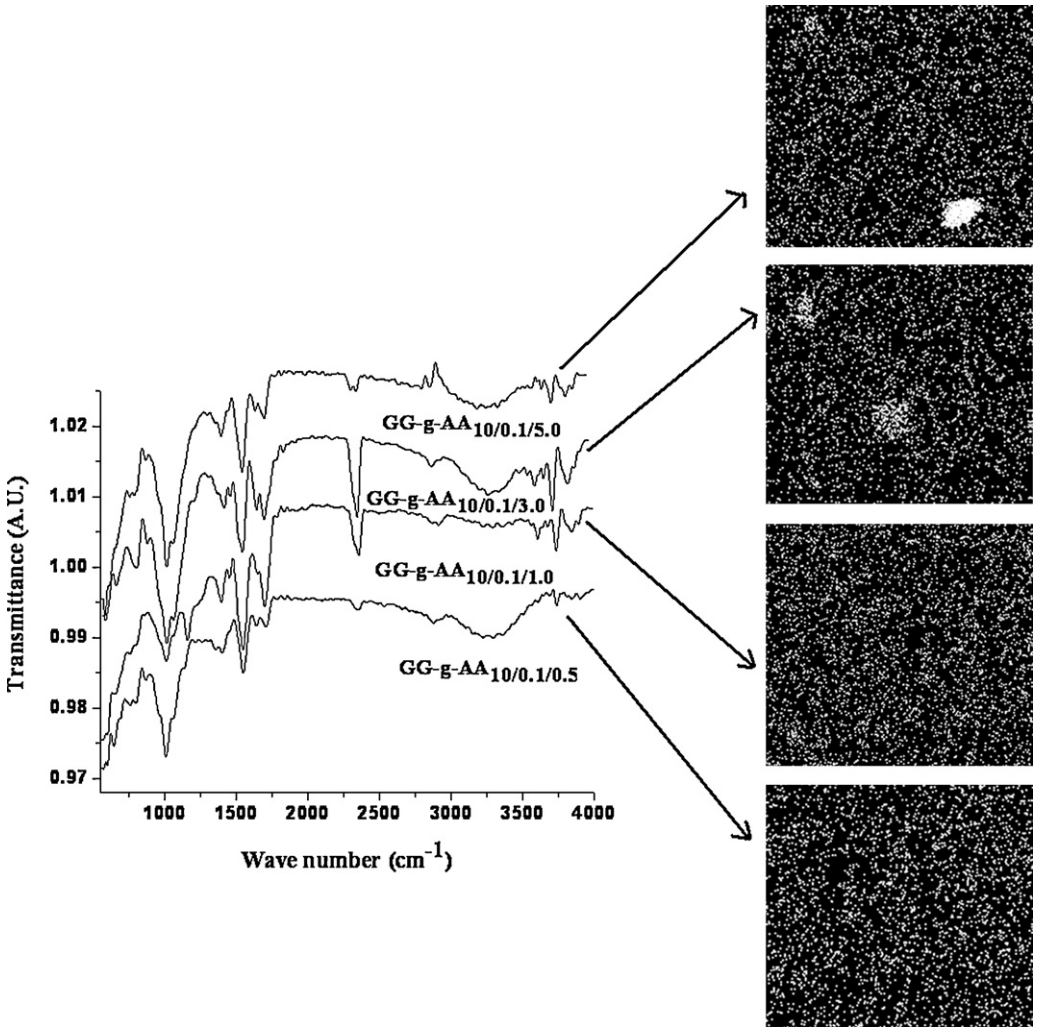

Fig. 4. Normalized FTIR spectra and subsequent EDX silica dot mapping of in situ grafted nanocomposites.

GG-g-$AA_{10/0.1}$ had shown extremely fast release kinetics with prominent bursting feature at the initial stage (Fig. 7b). Both these membranes were highly hydrophilic which adversely affected hydrophobic diclofenac retention potential, despite high viscosity. GG-g-$AA_{10/0.1}$ released nearly 48% of the loaded drug during the burst period followed by 28% in the second phase totaling to 76% elution after 20 h observation. However, GG had released 81% under identical condition. Conversely nanocomposite conjugates show more slow and sustained release (Fig. 7b). Maximum 52% diclofenac could be released from GG-g-$AA_{10/0.1/5.0}$ followed by 35% from GG-g-$AA_{10/0.1/3.0}$, 28% from GG-g-$AA_{10/0.1/0.5}$ and 24% from GG-g-$AA_{10/0.1/1.0.}$ Our previous best formulation with CMG–nanosilica (1 wt%) gave nearly 32% release, which is still 6% higher than our present slowest eluting composition (GG-g-$AA_{10/0.1/1.0}$). All conjugates except GG-g-$AA_{10/0.1/5.0}$ are free from bursting thus attributing better drug encapsulation as described in Fig. 5d. Kinetic data fitting in relevant models like zero order, first order, Higuchi and Korsmeyer–Peppas (power law) showed efficient fitting (r^2 values) in zero order, Higuchi and Korsmeyer–Peppas (power law) models (Table 1). Among these, Korsmeyer–Peppas model fitted best for all nanocomposites. The best formulation so far GG-g-$AA_{10/0.1/1.0}$, had shown nearly identical fitment with both zero order and Korsmeyer–Peppas kinetics which eventually implies that the release is more diffusion controlled (case I transport) vis-à-vis does not depend on the initial drug loading. Power law kinetic model is expressed in Eq. (2):

$$\frac{M_t}{M_\infty} = Kt^n \tag{2}$$

M_t is the mass concentration of diclofenac at various time intervals and M_∞ is the equilibrium release. K and n are constants. n predicts release mechanism. It is computed from the log–log plot (plot not shown in the article) of Eq. (2). The 'n' values are reported in Table 1. All 'n's were greater than 0.5 indicating "cage-relaxation" supported release mechanism of case I transport. The trend showed that more swellable samples had lower 'n' than those which were less swellable (exception GG-g-$AA_{10/0.1/0.5}$). Grafted units formed a cage-morphology which stimulated drug encapsulation but once the cage was swelled, it immediately released the drug which was the case with GG-g-$AA_{10/0.1}$. Conversely nanosilica provided more fix points (interaction) in the cage due to polymer adsorption (Fig. 5d). It improved encapsulation efficacy but high swelling tendency of the network still provided easy pathway for drug elution which happened in both GG-g-$AA_{10/0.1/3.0}$ and GG-g-$AA_{10/0.1/5.0}$ (Fig. 7c). GG-g-$AA_{10/0.1/0.5}$ displayed slower release despite high swelling possibly due to strong drug–nanosilica interaction. GG-g-$AA_{10/0.1/1.0}$ had been an outstanding composition, better than our previously designed CMG/nanosilica

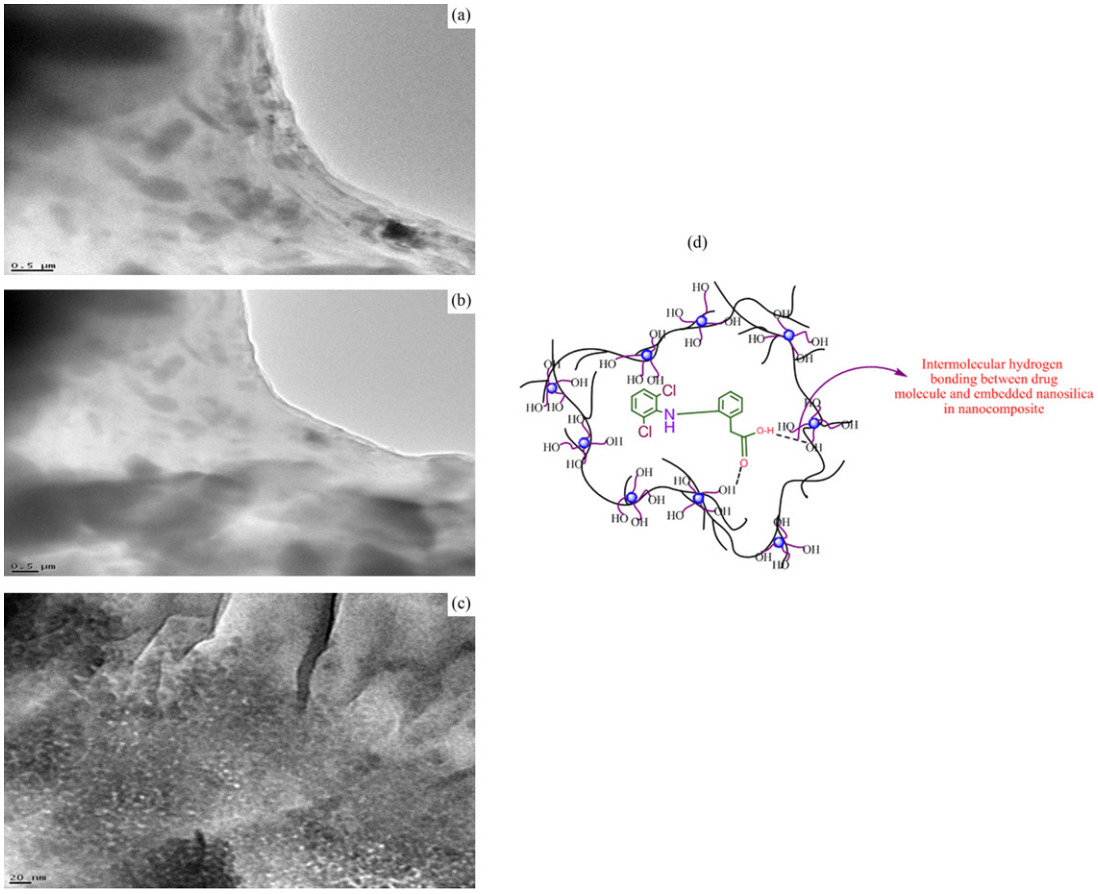

Fig. 5. TEM images of in situ grafted nanocomposites: (a) GG-g-AA$_{10/0.1/3.0}$, (b) GG-g-AA$_{10/0.1/5.0}$, (c) GG-g-AA$_{10/0.1/1.0}$ and (d) proposed schematic of copolymer/drug/nanosilica conjugate.

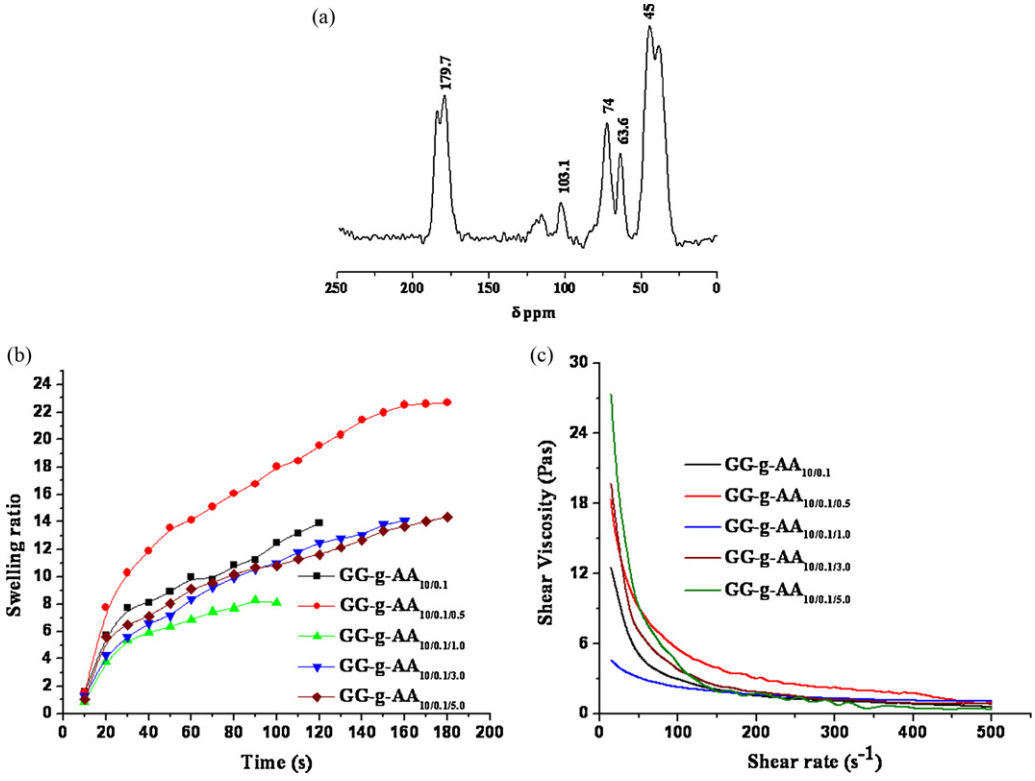

Fig. 6. (a) ^{13}C solid state NMR spectrum of representative GG-g-AA$_{10/0.1/1.0}$ and hydro-swelling kinetics (b) and shear rheological behavior (c) of GG-g-AA$_{10/0.1}$ and all its hybrid nanocomposites.

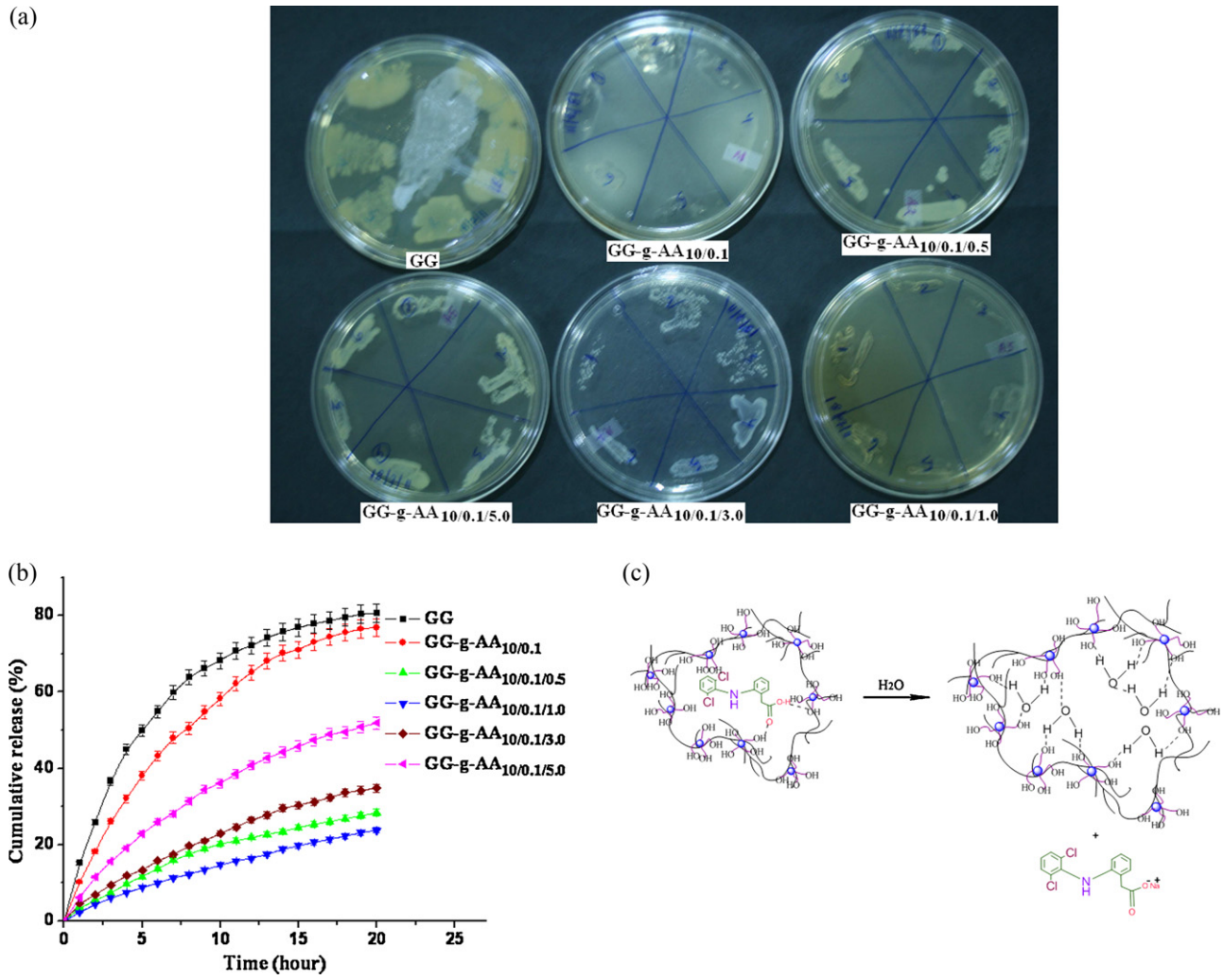

Fig. 7. (a) Microbial growth images after 72 h on virgin and other nanocomposites, (b) cumulative diclofenac release (in percent) kinetics of neat GG, GG-g-$AA_{10/0.1}$ and all of its nanocomposites (S.D. = ±3) and (c) elution of drug from copolymer/drug/nanosilica conjugate.

membrane (Giri et al., 2012), possibly due to higher hydrophobicity which sharply promoted the encapsulation efficacy. Highest *n* further implicated closeness to "ideal release" condition than else.

4. Conclusions

The graft–copolymer nanocomposites provided excellent control over diclofenac release due to high hydrophobicity and better cage morphology barring GG-g-$AA_{10/0.1/0.5}$, where the reason was better drug retention by the well dispersed nanosilica particles. Matrix–silica adhesion maximized at 1 wt% nanosilica content similar to our previously developed CMG/silica device, which was detected and proved using various analytical techniques. All nanocomposite conjugates had limited biocompatibility from which better skin compatibility and greater membrane life could be anticipated. Release profiles were preferably close to power law kinetics of the type shown in Eq. (2) in the text. The power law index close to 1 indicates ideally sustained release which was best suited for GG-g-$AA_{10/0.1/1.0}$. It leaves ample hope and aspiration for further investigation and trials in future using this composition in real field application.

Acknowledgement

The authors unanimously acknowledge financial support provided by the Centre for Research in Nanoscience and Nanotechnology (CRNN), University of Calcutta to carry out this work.

Appendix A. Supplementary data

Supplementary data associated with this article can be found, in the online version, at http://dx.doi.org/10.1016/j.carbpol.2012.08.035.

References

Adnadjevic, B., Jovanovic, J., & Drakulic, B. (2007). Isothermal kinetics of (E)-4-(4-metoxyphenyl)-4-oxo-2-butenoic acid release from a poly(acrylic acid) hydrogel. *Thermochimica Acta*, *466*, 38–48.

Altman, R., & Barkin, R. L. (2009). Topical therapy for osteoarthritis: Clinical and pharmacologic perspectives. *Postgraduate Medicine*, *121*, 139–147.

Butun, S., Ince, F. G., Erdugan, H., & Sahiner, N. (2011). One-step fabrication of biocompatible carboxymethyl cellulose polymeric particles for drug delivery systems. *Carbohydrate Polymers*, *86*, 636–643.

Banning, M. (2006). The use of topical diclofenac for pain in osteoarthritis of the knee: A review. *British Journal of Community Nursing*, *114*, 87–92.

Bhunia, T., Goswami, L., Chattopadhyay, D., & Bandyopadhyay, A. (2011). Sustained transdermal release of diltiazem hydrochloride through electronbeam irradiated different PVA hydrogel membranes. *Nuclear Instruments and Method in Physics Research B*, *269*, 1822–1828.

Bandyopadhyay, A., Bhowmick, A. K., & De Sarkar, M. (2004). Synthesis and characterization of acrylic rubber/silica hybrid composites prepared by sol–gel technique. *Journal of Applied Polymer Science*, *93*, 2579–2589.

Bandyopadhyay, A., De Sarkar, M., & Bhowmick, A. K. (2005). Polymer–filler interactions in sol–gel derived polymer/silica hybrid nanocomposites. *Journal of Polymer Science Part B: Polymer Physics*, *43*, 2399–2412.

Cavalieri, F., Chiessi, E., Villa, R., Vigano, L., Zaffaroni, N., Telling, F. M., et al. (2008). Novel PVA-based hydrogel microparticles for doxorubicin delivery. *Biomacromolecules*, *9*, 1967–1973.

Don, T. M., Huang, M. L., Chiu, A. C., Kuo, K. H., Chiu, W. Y., & Chiu, L. H. (2008). Preparation of thermo-responsive acrylic hydrogels useful for the application in transdermal drug delivery systems. *Materials Chemistry and Physics*, *107*, 266–273.

El-Leithy, E. S., Shaker, D. S., Ghorab, M. K., & Abdel-Rashid, R. S. (2010). Evaluation of mucoadhesive hydrogels loaded with diclofenac sodium–chitosan microspheres for rectal administration. *AAPS PharmSciTech*, *11*, 1695–1702.

Frutos, G., Prior-Cabanillas, A., París, R., & Quijada-Garrido, I. (2010). A novel controlled drug delivery system based on pH-responsive hydrogels included in soft gelatin capsules. *Acta Biomaterialia*, *6*, 4650–4656.

George, M., & Abraham, T. E. (2007). pH sensitive alginate–guar gum hydrogel for the controlled delivery of protein drugs. *International Journal of Pharmaceutics*, *335*, 123–129.

Giri, A., Bhowmick, M., Pal, S., & Bandyopadhyay, A. (2011). Polymer hydrogel from carboxymethyl guar gum and carbon nanotube for sustained trans-dermal release of diclofenac sodium. *International Journal of Biological Macromolecules*, *49*, 885–893.

Giri, A., Ghosh, T., Panda, A. B., Pal, S., & Bandyopadhyay, A. (2012). Tailoring carboxymethyl guargum hydrogel with nanosilica for sustained transdermal release of diclofenac sodium. *Carbohydrate Polymers*, *87*, 1532–1538.

Huang, Y., Yu, H., & Xiao, C. (2007). pH-sensitive cationic guar gum/poly (acrylic acid) polyelectrolyte hydrogels: Swelling and in vitro drug release. *Carbohydrate Polymers*, *69*, 774–783.

Krishnaiah, Y. S. R., Karthikeyan, R. S., & Satyanarayana, V. (2002). A three-layer guar gum matrix tablet for oral controlled delivery of highly soluble metoprolol tartrate. *International Journal of Pharmaceutics*, *241*, 353–366.

Lee, W. F., & Chen, Y. C. (2006). Effects of intercalated hydrotalcite on drug release behavior for poly(acrylic acid-co-*N*-isopropyl acrylamide)/intercalated hydrotalcite hydrogels. *European Polymer Journal*, *42*, 1634–1642.

Morrow, D. I. J., McCarron, P. A., Woolfson, A. D., Juzenas, P., Juzeniene, A., Iani, V., et al. (2010). Novel patch-based systems for the localised delivery of ALA-esters. *Journal of Photochemistry and Photobiology B: Biology*, *101*, 59–69.

McCoy, C. P., Morrow, R. J., Edwards, C. R., Jones, D. S., & Gorman, S. P. (2007). Neighboring group-controlled hydrolysis: Towards designer drug release biomaterials. *Bioconjugate Chemistry*, *18*, 209–215.

Onuki, Y., Nishikawa, M., Morishita, M., & Takayama, K. (2008). Development of photocrosslinked polyacrylic acid hydrogel as an adhesive for dermatological patches: Involvement of formulation factors in physical properties and pharmacological effect. *International Journal of Pharmaceutics*, *349*, 47–52.

Prabaharan, M. (2011). Prospective of guar gum and its derivatives as controlled drug delivery systems. *International Journal of Biological Macromolecules*, *49*, 117–124.

Sullad, A. G., Manjeshwar, L. S., & Aminabhavi, T. M. (2010). Novel pH-sensitive hydrogels prepared from the blends of poly (vinyl alcohol) with acrylic acid-graft-guar gum matrixes for isoniazid delivery. *Industrial and Engineering Chemistry Research*, *49*, 7323–7329.

Santos, H., Veiga, F., Pina, M. E., & Sousa, J. J. (2005). Compaction, compression and drug release properties of diclofenac sodium and ibuprofen pellets comprising xanthan gum as a sustained release agent. *International Journal of Pharmaceutics*, *295*, 15–27.

Thakur, S., Chauhan, G. S., & Ahn, J. H. (2009). Synthesis of acryloyl guar gum and its hydrogel materials for use in the slow release of L-DOPA and L-tyrosine. *Carbohydrate Polymers*, *76*, 513–520.

Tortora, M., Cavalieri, F., Chiessi, E., & Paradossi, G. (2007). Michael-type addition reactions for the in situ formation of poly(vinyl alcohol)-based hydrogels. *Biomacromolecules*, *8*, 209–214.

Tomic, S. L., Micic, M. M., Dobic, S. N., Filipovic, J. M., & Suljovrujic, E. H. (2010). Smart poly (2-hydroxyethyl methacrylate/itaconic acid) hydrogels for biomedical application. *Radiation Physics and Chemistry*, *79*, 643–649.

Wang, A. G., Xia, T., Yuan, J., Yu, R. A., Yang, K. D., Chen, X. M., et al. (2004). Effects of phenobarbital on metabolism and toxicity of diclofenac sodium in rat hepatocytes in vitro. *Food and Chemical Toxicology*, *42*, 1647–1653.

Yu, X., & Pishko, M. V. (2011). Nanoparticle-based biocompatible and targeted drug delivery: Characterization and in vitro studies. *Biomacromolecules*, *12*, 3205–3212.

Zhou, Y., & Faust, R. (2005). Syntheses and characterization of poly(cyclohexyl vinyl ether-stat-vinyl alcohol)-b-polyisobutylene-b-poly(cyclohexyl vinyl ether-stat-vinyl alcohol)triblock copolymers and their application as coatings to deliver paclitaxel from coronary stents. *Macromolecules*, *38*, 8183–8191.